DOI: 10.1590/2317-4889201820170130

ARTICLE

Emerald from the Fazenda Bonfim Deposit, northeastern Brazil: chemical, fluid inclusions and oxygen isotope data

Judiron Santos Santiago[1,2]*, Valmir da Silva Souza[1,3], Bernardo de Carvalho Filgueiras[1,4], Federico Alberto Cuadros Jiménez[1,3]

ABSTRACT: *The Fazenda Bonfim emerald deposit, State of Rio Grande do Norte, is within the regional geological domain known as Seridó Mobile Belt, Borborema Tectonic Province. It was formed from metasomatic fluids interaction at along lithological contacts between Be-rich albite-granite intrusions and Cr (±V)-rich mafic-ultramafic host-rocks, enclosed in the lens-shaped "hornfels" phlogopite schist. Emerald crystals display relatively high contents of Mg and Na, as well as trace amounts of Ca, K, Cs, Li, P, Sc, Ti, Mn, Co, Ni, Zn, Ga and Rb. Cr is the main chromophore element, followed by Fe and some V. Display also concentric growth zones and randomly-oriented mineral micro-inclusions, indicative for static growth. This zoning is linked to cationic substitution of alkalis accompanied by Cr loss, which favors irregular coloration of crystals. Metasomatic fluids contemporaneous with emerald growth are aqueous (H_2O+NaCl), with low to moderate salinity and low density, although trace amounts of CO_2 ± CH_4 were also observed. These fluids showed a field-trapped between 375–430ºC and 200–600 bars, based on combination of fluid inclusions isochores. In addition, oxygen isotope data ($\delta^{18}O$ = 6.9–7.4‰) suggest an igneous-metasomatic source for fluids and emerald components.*

KEYWORDS: *Fazenda Bonfim Emerald Deposit; Seridó Mobile Belt; Borborema Tectonic Province; Chemical Mineral; Fluid Inclusions; Oxygen Isotope.*

INTRODUCTION

The northeastern Brazil region hosts beautiful and exotic varieties of gem-quality mineral occurrences linked to different generations of granitic pegmatite bodies related to the Brasiliano orogeny (800–500 Ma; according to Brito Neves *et al.* 2014). These pegmatites are essentially composed of quartz, muscovite, microcline and albite, and may contain economical amounts of beryl, spodumene, cassiterite, columbite-tantalite, tourmaline and other minerals, crystallized between 550 and 350ºC at 3.0–3.5 kb (Johnston Jr. 1945, Cassedanne 1991, Silva *et al.* 1995, Araújo *et al.* 2001, Beurlen *et al.* 2001, Baumgartner *et al.* 2006, Angelim *et al.* 2006, Cavalcante *et al.* 2016). In this region, emerald deposits of economic importance are known since the mid-twentieth century, especially in the State of Bahia, but less important deposits are also registered in the Ceará and Rio Grande do Norte States. These deposits resulted from metasomatic interaction between granitic pegmatite fluids and metavolcano-sedimentary rocks, mainly basic-ultrabasic composition or their metamorphic equivalents, affected by complex folding and deformation (Giuliani *et al.* 1990, Agrawal 1992, Beurlen *et al.* 2009, Oliveira & Ali 2011).

The Fazenda Bonfim emerald deposit is located in the central portion of the State of Rio Grande do Norte, within the Seridó Mobile Belt domain, in the Borborema Tectonic Province (Fig. 1). This deposit is located at Universal Transverse Mercator (UTM) coordinates 819134/9353574 (zone 24M)

[1]Programa de Pós-Graduação em Geologia, Instituto de Geociências, Universidade de Brasília – Brasília (DF), Brazil. *E-mails: judirongeo@yahoo.com.br, valmirsouzaunb@gmail.com, bernardocfilgueiras@gmail.com, facuadros@unb.br*

[2]Companhia Baiana de Pesquisa Mineral – Salvador (BA), Brazil.

[3]Instituto de Geociências, Universidade de Brasília – Brasília (DF), Brazil.

[4]Votorantim Metais – Goianésia (GO), Brazil.

*Corresponding author

Manuscript ID: 20170130. **Received on:** 10/31/2017. **Approved on:** 02/19/2018.

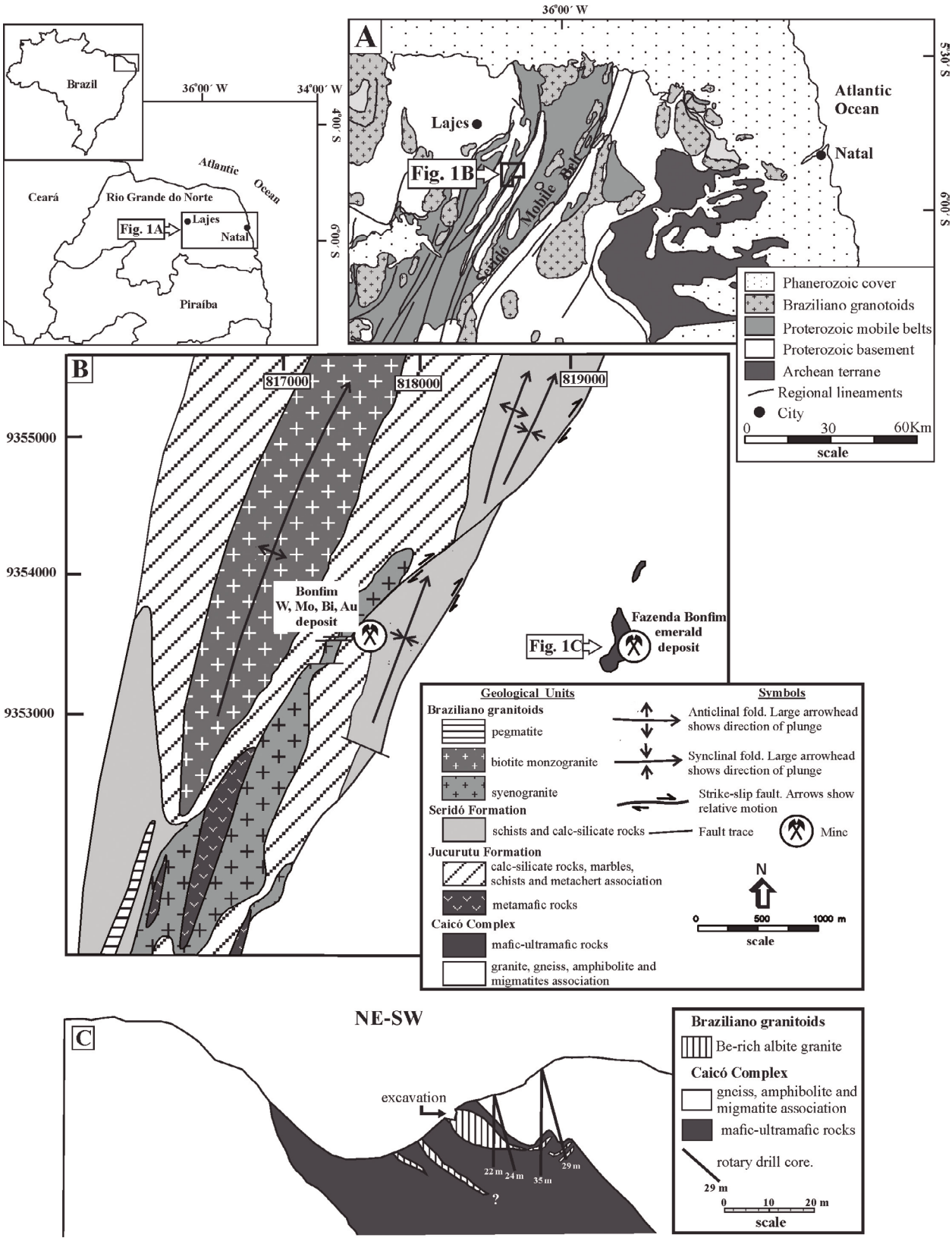

Figure 1. Geological and location maps of the Fazenda Bonfim emerald deposit. (A) Regional geological subdivision map (adapted from Cavalcante Neto & Barbosa 2007); (B) local geological map. Observe the distribution of W, Mo, Bi, Au and emerald deposits in the area (adapted from Nosso Senhor do Bonfim Mining Company internal report); (C) geological cross-section of the excavation area of the mine inferred from geological mapping and borehole data. The vertical scale is exaggerated (Santiago 2017).

and was discovered at the end of year of 2005 during mineral prospecting for Cr and Ni associated with ultramafic rocks. Currently, the Vale Verde Mining Company, which holds the exploration rights, is reassessing the mine in order to resume production. According to Brasil (2017), around 300 kg of emerald was commercialized by Rio Grande do Norte at 2016, making over US$ 12,000. However, this region is geochemically anomalous for Cr, Be, K and Li, as well as for Mg, Na, Ni and V, which are favorable for the occurrence of additional emerald deposits (Scholz *et al*. 2010).

In the Fazenda Bonfim deposit, emeralds occur at the contact between Be-rich granitic body and ultrabasic rocks, mainly enclosed in irregular lens-shaped of phlogopite schist. At this site, gems typically consist of short crystals with concentric growth zones ranging from light bluish green to medium-dark bluish green, and chemical composition characterized by relatively high amounts of Mg, low Na and traces of Ca, K, Cs, Li, P, Sc, Ti, Mn, Co, Ni, Zn, Ga, Rb, Cr, Fe and V (Cavalcante Neto & Barbosa 2007, Zwaan *et al*. 2012, Santiago 2017). In this paper, we present new data on the chemical, oxygen isotope and fluid inclusions compositions about emerald crystals from the Fazenda Bonfim deposit, thus increasing our knowledge on the formation of emeralds linked to generations of granitic bodies during the Neoproterozoic Brasiliano orogeny in the northeastern Brazil.

ANALYTICAL METHODS

Conventional petrographic and electron microscope investigations were carried out at the Geoscience Institute of the University of Brasília. A FEI (QUANTA — 450 model) electron microscope was used to image of polished thin sections, which were previously coated with carbon. This microscope was equipped with a high-performance EDAX EDS/SDD spectrometer system. Imaging of minerals was achieved via acquisition of mixed signals of both backscattered (BSE) and transmitted (TE) electrons. The electron spectra were acquired using a working distance of 10 mm for 10–20 s of clock time, with probe size varying between 0.1 and 0.2 nm, and beam current and accelerating voltage of 400–500 pA and 20 kV, respectively.

Chemical analyses of emerald crystals were obtained via electron probe microanalysis techniques (EPMA) at the Geoscience Institute of the University of Brasília, using a JEOL JXA-8230 microanalyzer with five coupled wavelength dispersive spectrometers (WDS), under the supervision of Prof. Dr. N. F. Botelho. Conditions used during analyses consisted of accelerating voltage of 20 kV, beam current of 40 nA, beam diameter of 1–2 μm, and counting times of 15 and 10 s for peak and background positions, respectively.

The fluid inclusion study was conducted on six double-polished samples of emerald crystals with sizes between 0.4 and 1.2 cm. After conventional petrographic analysis, microthermometric measurements were carried out using a LINKAM THMSG-600 heating-freezing system coupled to an Olympus BX-51 petrographic microscope with 40x and 100x long distance objectives at the Geoscience Institute of the University of Brasília. Calibration of the stage was performed using synthetic fluid inclusion standards, applying speed rates around 1ºC/min, with an estimated accuracy of ± 0.5ºC for the freezing stage (+25º to -100ºC) and ± 5ºC for the heating stage (maximum temperature of 500ºC). In addition, laser Raman spectroscopic analyses were performed using a HORIBA Jobin Yvon SPEX T64000 series spectrometer, with a Symphony II multichannel detector coupled to an Olympus BX-51 microscope at the Physics Institute of the University of Brasília. The light source consisted of a Coherent krypton/argon ion laser with a wavelength of 532 nm and irradiation time of 10 s. Calibration was carried out using a silicon standard. Data processing was achieved using Origin 6.0 software.

Oxygen isotope ratio ($^{18}O/^{16}O$) measurements on three emerald samples and three quartz samples were conducted at the National Isotope Centre laboratories, New Zealand, under the supervision of Prof. Dr. Kevin Faure. Nearly pure emerald and quartz crystals were handpicked from selected specimens. Oxygen was extracted from sample powder using a CO_2-laser (Sharp 1990). Oxygen isotope-ratio values are reported in the familiar $\delta^{18}O$ notation, relative to Vienna Standard Mean Ocean Water (VSMOW). Samples were normalized to the international quartz standard NBS-28 using a value of +9.6 per mil (‰). Four analyses of the NBS-28 standard were carried out during the same analytical sessions of samples, yielding values that varied by less than 0.15‰. Samples and standards were heated overnight to 150ºC before loading them into the vacuum extraction line during approximately 6 hours. Blank BrF_5 runs were carried out until they yielded less than 0.2 μ moles of oxygen. Oxygen yields were recorded along with CO_2 gas analyses using a Geo20-20 mass spectrometer.

GEOLOGICAL SETTING

A large part of northeastern Brazil lies within the Borborema Tectonic Province (Almeida *et al*. 1981), formed from aggregation of several crustal blocks during Paleo- to Mesoproterozoic times, and subsequently restructured during the late Neoproterozoic Brasiliano orogeny (Caby *et al*. 1991, Jardim de Sá *et al*. 1995, Van Schmus *et al*. 1995, Brito Neves *et al*. 2000, Neves 2003). During the Brasiliano orogeny, a strong strike-slip dynamic led to

generation of dextral wrench/strike-slip fault systems that divided the Borborema Province into different domains or terranes (Fig. 1A). In this geotectonic context, the State of Rio Grande do Norte is divided into the Jaguaribeano, Rio Piranhas-Seridó and São José do Campestre domains. In addition, Cretaceous and Paleogene/Neogene sedimentation along with basic magmatism took place in the area as well (Angelim *et al.* 2006). The emerald deposits are located within the Rio Piranhas-Seridó domain, in the context of the Neoproterozoic Seridó Mobile Belt (Fig. 1A).

The Archean-Paleoproterozoic basement of Seridó Mobile Belt is composed of migmatite, granite-gneiss, metagranitoid, amphibolite, metamafic-metaultramafic rocks and metavolcano-sedimentary sequences grouped within two regional units known as São José de Campestre Massif and Caicó Complex (Jardim de Sá 1994, Dantas 1997, Dantas *et al.* 2013, Souza *et al.* 2007). On top of the basement, Neoproterozoic supracrustal units making up the Seridó Group were deposited, which is composed of diverse metasedimentary sequences, subdivided, from base to top, into the Jurucutu, Equador and Seridó formations (Angelim *et al.* 2006, Van Schmus *et al.* 2003, Caby *et al.* 1995).

Basement rocks and Seridó Group units were intruded by Neoproterozoic pre- to post-Brasiliano orogeny granitic magmas with a clear tectonic control. This voluminous Brasiliano magmatism (580–570 Ma) is divided into several suites, consisting of medium to coarse-grained granitoids and Be-Ta-Li-Sn, gem-bearing pegmatite bodies (Baumgartner *et al.* 2006). These rocks present variable degrees of deformation and include an expanded granitoid series ranging from gabbro/diorite to alkali-feldspar syenogranite/syenite, and rare albite-granite (Jardim de Sá *et al.* 1981, Sial 1986, Ferreira *et al.* 1998, Nascimento *et al.* 2000). Tectonically controlled W -Mo -Bi ± Au skarn deposits often develop at the contact zone between Brasiliano granitoids and Seridó Group marble or calc-silicate rocks (Fig. 1B). On the other hand, emerald mineralizations occasionally occur at the contact zone between granitoids and Caicó Complex mafic-ultramafic rocks bodies (Silva *et al.* 1995, Angelim *et al.* 2006, Cavalcanti *et al.* 2016, Souza Neto *et al.* 2008).

LOCAL GEOLOGY

The Fazenda Bonfim emerald deposit lies within the Caicó Complex basement (Fig. 1B). In this site, this complex is mainly composed of orthogneiss, augen gneiss and interfingered amphibolite lenses, as well as mafic-ultramafic lenticular bodies. The excavation face was developed at the contact between lenticular mafic-ultramafic and Be-rich albite granite bodies (Figs. 1C and 2A).

Mafic-ultramafic lenticular bodies are deeply serpentinized and exhibit pod geometry dipping 40–45º to NW with internal complex structural arrangement, marked by distinct foliation types and fold generation. Petrographic study is complicated due to the advanced serpentinization, but four basic petrographic types have been identified: tremolite-talc-serpentine schist, tremolite-phlogopite schist, talc-serpentine schist and actinolite-phlogopite schist. Most of the studied samples show mesh and bastite/fibrous microtexture, defined by fine-grained talc, serpentine and tremolite with few relics/skeletal of olivine or pyroxene phenocrysts. On the other hand, Brasiliano medium to coarse-grained granite lenticular bodies show white to off-white cream color, deformation concentrated at the edges with undeformed cores, and contain disseminated euhedral to subhedral beryl crystals. It consists of granoblastic to heterogranular albite granite composed essentially of albite (An_{4-8}), quartz and muscovite, with rare interstitial microcline. Zircon, apatite, opaque minerals, Fe-oxide and white-mica occur as accessories.

Emerald is mainly contained within irregular lens-shaped coarse-grained phlogopite schist, formed from metasomatic interaction between mafic-ultramafic rocks and albite granite fluids (Figs. 2B), which may be identified as phlogopite hornfels, and it is also referred to as "blackwall" zone in other emerald deposits of the world (*e.g.*, Grundmann & Morteani 1989, Andrianjakavah *et al.* 2009). Phlogopite schist is composed almost entirely of euhedral to subhedral phlogopite aggregates, usually larger than 5 mm, surrounding emerald crystals (Fig. 2C). However, sugary quartz-veinlets containing emerald crystals often occur.

EMERALD CHEMICAL COMPOSITION

The emerald crystals show euhedral to subhedral habits, color ranging from light bluish green to medium-dark bluish green, light zoning and slight to moderate fracturing (Fig. 2C). BSE imaging reveals a discreet concentric zoning and some randomly oriented micro-inclusions (zircon, monazite and mica), which indicates static growth (Fig. 2D). In addition, Zwaan *et al.* (2012) also identified micro-inclusions of sodic plagioclase, phlogopite, hematite and quartz.

Representative electron-microprobe analyses intervals for around 130 different spots are shown in Table 1, whose results are reported as wt.% oxide. The analyses were usually carried out perpendicular to the *c*-axis and following color zoning (edge to edge). Number of ions in mineral formula were calculated on the basis of 18 and 3 O and Be atoms, respectively, per formula unit (apfu), while the H_2O content was calculated applying the equation proposed by Marshall *et al.* (2016) This stoichiometric approach is useful because

of the difficulty in obtaining accurate analytical results for Be (Groat *et al.* 2002). The sum of the oxides is usually below 100 wt.%, commonly between 97 and 99 wt.%, which is presumably linked to the accuracy in the stoichiometric calculation of Be and H_2O. In general, these intervals of chemical composition are relatively consistent with the data presented by Zwaan *et al.* (2012).

The most important chromophore element is Cr, followed by Fe and some V. Furthermore, it is important to note the elevated contents of Mg and Na. According to Zwaan *et al.* (2012), LA-ICP-MS analyses of emeralds from Fazenda Bonfim yielded trace amounts of Ca, K, Cs, Li, P, Sc, Ti, Mn, Co, Ni, Zn, Ga and Rb.

The beryl/emerald structure is made up of hexagonal rings of SiO_4 tetrahedra stacked parallel to the *c* crystallographic axis, and crosslinked by Be tetrahedra and Al octahedra. Channel-like cavities parallel to the *c*-axis that result from ring stacking may host alkalis, H_2O and CO_2 molecules, as well as Li, Cr, Fe and other trace elements (Gibbs *et al.* 1968, Morosin 1972, Artioli *et al.* 1993). The electron probe microanalyses indicate that $[Si_6O_{18}]$ hexagonal rings of the Fazenda Bonfim emerald crystals are slightly Si-deficient (Si < 6 apfu) (Tab. 1), which must be accompanied by the entrance of Al^{3+} or some Be^{2+} in the tetrahedral sites (Aurisicchio *et al.* 1988, Ferraris *et al.* 1998). On the other hand, the octahedral Al-site also shows Al^{3+} deficiency (Al = 1.49 to 1.66 apfu, Tab. 1), thus allowing accommodation of Cr, Fe and Mg cations. This occupancy of octahedral Al-site is demonstrated by a negative correlation observed between Al and Fe + Mg + Cr (Fig. 3A), which defines a common cationic substitution taking place within the beryl octahedral sites (*e.g.*, Sampaio Filho *et al.* 1973, Abdalla & Mohamed 1999, Vapnik *et al.* 2006). In this cationic substitution, alkalis (Na and K) and H_2O have an important role in maintaining the charge balance of the structure (Groat *et al.* 2002). These compensating substitutions may be responsible for the chemical zoning observed in the emerald crystals, varying from the core towards the rim. The entrance of these compensating cations is indicated by positive correlation between the sums Mg + Fe and Na +

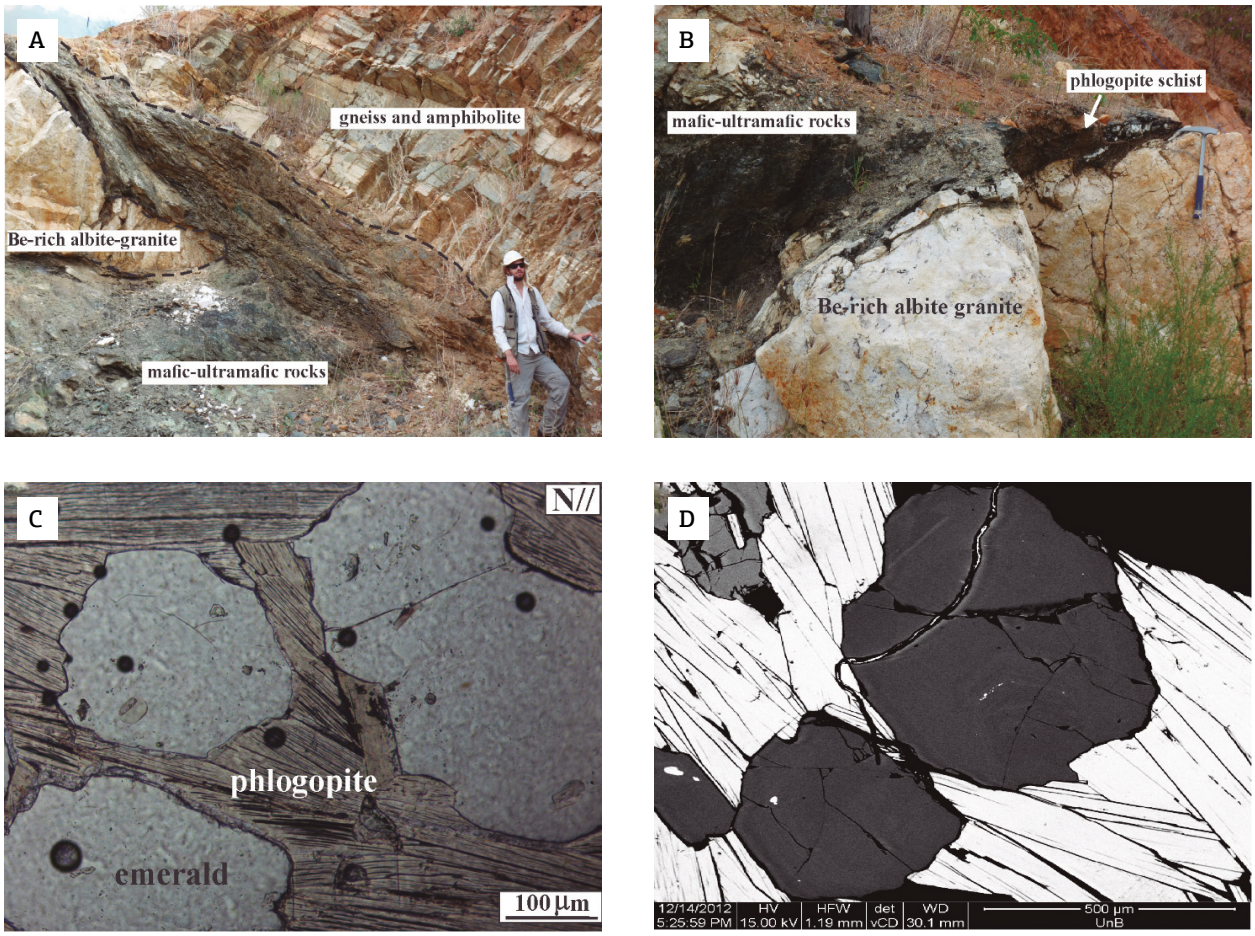

Figure 2. (A) Main wall-rock types in the excavation area of the Fazenda Bonfim emerald deposit; (B) irregular lens-shaped, emerald-bearing phlogopite schist located at the contact between mafic-ultramafic rocks and pegmatitic albite granite; (C) photomicrography of emerald crystals contained within phlogopite schist (N// = parallel polars); (D) back-scattered electron image of zoned emerald crystals with some mineral micro-inclusions.

K + Rb (Fig. 3B). In this diagram, the data plot above the correlation straight-line (1:1), which suggests, according to Groat *et al.* (2002, 2008), the presence of Li^{+} substituting Be^{2+} at the Be-site. According to Zwaan *et al.* (2012), the Li-content of the Fazenda Bonfim emerald crystals vary from 70 to 130 ppm.

Table 1. Intervals of electron-microprobe analysis results around 130 different spots obtained from the Fazenda Bonfim emerald crystals. The number of ions in mineral formula were calculated on the basis of 3 Be and 18 O.

Elements	Average	Minimum	Maximum
SiO_2 (wt.%)	64.75	63.30	66.55
Al_2O_3	14.83	13.63	15.50
FeO_{total}	0.65	0.49	0.84
Cr_2O_3	0.57	0.11	1.70
MgO	2.24	1.87	2.70
MnO	0.01	0.00	0.05
CaO	0.02	0.00	0.08
Na_2O	1.76	1.52	2.10
K_2O	0.03	0.00	0.07
Rb_2O	0.14	0.00	0.27
Cs_2O	0.03	0.00	0.14
V_2O_5	0.03	0.00	0.12
BeO*	13.48	13.17	13.84
H_2O**	2.49	2.41	2.59
Total	101.04	99.07	103.57
Si^{4+} (apfu)	5.99	5.96	6.02
$^{IV}Al^{3+}$	0.00	0.00	0.04
Si (tetrahedra) sum	6.00	6.00	6.02
$^{VI}Al^{3+}$	1.61	1.49	1.66
Cr^{3+}	0.04	0.01	0.13
Fe^{2+}	0.05	0.04	0.07
Mn^{2+}	0.00	0.00	0.00
Mg^{2+}	0.31	0.26	0.37
Ca^{2+}	0.00	0.00	0.01
Na^{+}	0.32	0.27	0.37
V^{5+}	0.00	0.00	0.02
K^{+}	0.00	0.00	0.01
Rb^{+}	0.01	0.00	0.02
Be^{2+}***	3.00	3.00	3.00

*Stoichiometric calculation; **calculated using the equation H_2O = (0.5401 × lnNa_2O) + 2.1867 (Marshall *et al.* 2016); ***ideal value for stoichiometric calculations.

Ternary correlation diagrams (Figs. 3C and 3D), applied for all the analyzes obtained, consisting of main oxides of elements that participate in octahedral Al-site substitutions (FeO-MgO-Cr_2O_3), and oxides of chromophore elements in emerald (FeO-Cr_2O_3-V_2O_3), as pointed by Groat *et al.* (2002), show that Mg was the main substituent in the Fazenda Bonfim emerald crystals, while Fe and Cr were main elements responsible for variation in color. These diagrams also show for comparison the compositional field of other Brazilian emerald deposits, which present a geological context similar to that of the Fazenda Bonfim emerald deposit, and whose data are available in the literature.

Data of selected oxides in emerald along a crystal profile with spots approximately equidistant to each other (Fig. 3E) revealed that Na tends to maintain proportional to Mg content (Fig. 3F), depicting the role of alkalis in favoring the chemical zoning and irregular coloration of crystals. In this context, excess charge is then balanced by the coupled substitution of alkalis (mainly Na) in the channel sites, along with H_2O (Laurs *et al.* 1996). The reason for this type of zoning is not yet clear, but it is possible that some degree of chemical imbalance within the environment of growth is the main factor. On the other hand, Cr content presents strong oscillation along a crystal profile, while Fe content exhibits little variation and the very low V content remains constant. Therefore, it is probable that Cr loss also contributed for the changes in color of the Fazenda Bonfim emerald crystals, which show pale green hues.

FLUID INCLUSIONS

Only fluid inclusions from emerald crystals were studied in this work. Forty-seven aqueous-type fluid inclusions observed at room temperature (± 20ºC) were essentially primary, with very few fluid inclusions displaying an aqueous-carbonic character. Emerald crystals exhibit some microfractures that contain fluid inclusions less than 20 µm in size, which were classified as secondary or pseudo-secondary.

Petrography

At room temperature, primary aqueous-type fluid inclusions are arranged in groups parallel to the crystal growth zones. They are composed of three types:

- type 1: fluid inclusions of this type present elongated to cylindrical shapes, and range between 40 and 70µm in size. They are mainly composed of two immiscible phases ($H_2O_{(gas)}$ + $H_2O_{(liquid)}$), although some inclusions

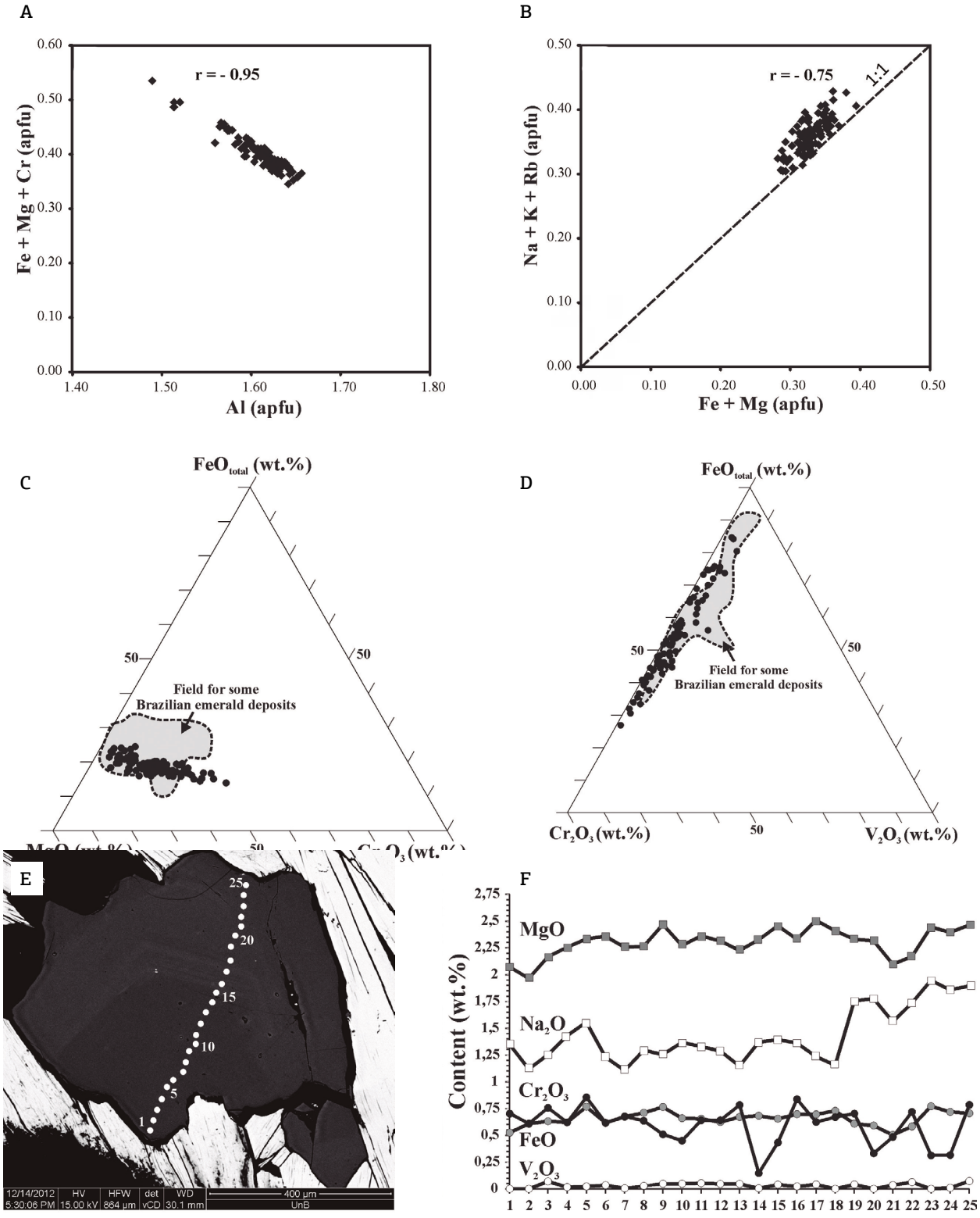

Figure 3. Correlation diagrams of the Fazenda Bonfim emerald crystals (adapted from Groat *et al.* 2002). (A) Al *vs.* Fe + Mg + Cr (apfu); (B) Mg + Fe *vs.* Na + K + Rb (apfu); (C) FeO-MgO-Cr_2O_3 (wt.%); (D) FeO-Cr_2O_3-V_2O_3 (wt.%). The gray, dotted-contoured field in (C) and (D), represents chemical compositions of some Brazilian emeralds (data compiled from Schwarz 1987); (E) back-scattered electron image of zoned emerald crystals, indicating the position of the transverse electron microprobe chemical analysis spots spaced equidistantly; (F) weight percent data for some selected oxides in emerald along a traverse.

having only one H_2O_{liquid} phase are also present (Fig. 4A and 4B). Volume fractions of the gas phase (Vg/Vt) vary from 0 to 60%. Occasionally, two-phase inclusions of this type host daughter minerals less than 5 µm in size, commonly displaying from sub-rounded to irregular shapes, colorless to slightly pink hues and low to moderate birefringence. Opaque daughter minerals are also found within these inclusions;

- type 2: these fluid inclusions vary between 90 and 100 µm in size, show acicular shapes, and are essentially composed of $H_2O_{(gas)}$ + $H_2O_{(liquid)}$ (Fig. 4A). Volume fractions (Vg/Vt) vary from 15 to 25%, and, in some samples, daughter minerals around 1 µm in size are also observed;
- type 3: fluid inclusions grouped in this category are the most abundant in the studied samples, show from cubic to rectangular shapes, and range between 50 and 70 µm in size. These inclusions are composed either of two or three immiscible phases, namely $H_2O_{(gas)}$ + $H_2O_{(liquid)}$, or $H_2O_{(gas)}$ + $H_2O_{(liquid)}$ + solid (Fig. 4C). Vg/Vt ratios vary from 30 to 50%, while colorless daughter minerals present sub-rounded shapes, moderate birefringence, and are between 1 and 5 µm in size. Opaque daughter minerals are also observed within this type of fluid inclusion.

During petrographic study, we identified only six primary aqueous carbonic-type fluid inclusions (Type 4), which occur in a discrete manner and present sub-rounded to ellipsoidal shapes with diameter varying between 20 and 35 µm. Such fluid inclusions are composed of a H_2O-CO_2 mixture distributed into three immiscible phases: two liquid phases and one gas phase (Fig. 4D). Volume fractions of the gas phase in type-4 fluid inclusions varies between 30 and 40%. On the other hand, according to Zwaan *et al.* (2012), FTIR spectroscopy investigations indicated considerable presence of CO_2 and deuterated water at Fazenda Bonfim emeralds.

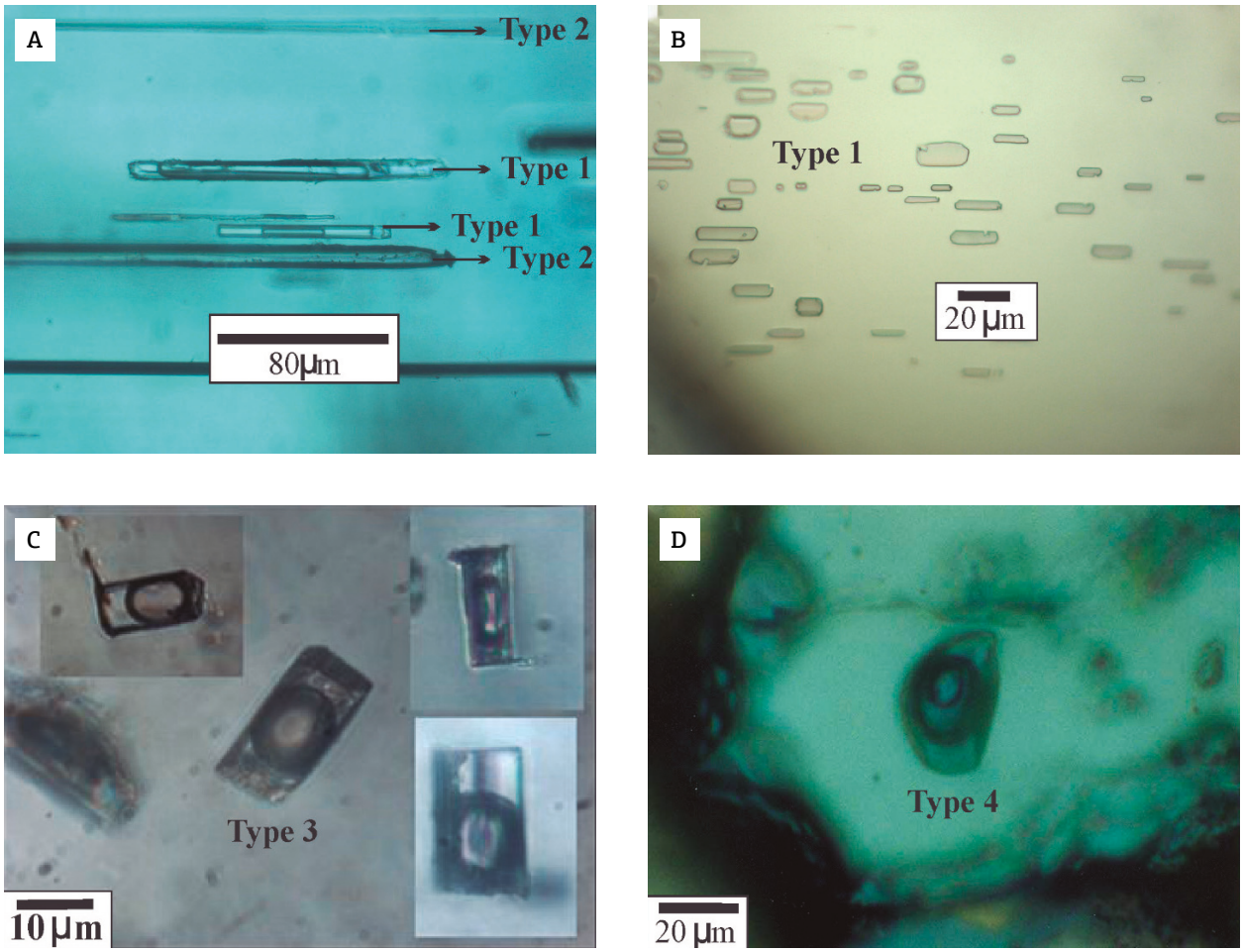

Figure 4. Morphological features of main fluid inclusion types identified in the Fazenda Bonfim emerald crystals. (A) Types 1 and 2 aqueous fluid inclusions displaying elongated or acicular shapes; (B) variation of type 1 fluid inclusions having monophase constitution; (C) type 3 aqueous fluid inclusions displaying cubic to prismatic shapes; (D) rare type 4 aqueous-carbonic fluid inclusion.

Microthermometry

Results of microthermometric measurements has its intervals showed and discussed as follows. Density values were calculated using MacFlinCor software (Brown & Hagemann 1994). For aqueous fluid inclusions, salinities were estimated from ice final melting temperatures (Tm ice), using the equation proposed by Bodnar (1993). For aqueous-carbonic fluid inclusions, salinity values were calculated from clathrate final melting temperatures (Tm clath), using the equations proposed by Diamond (1992) and Bakker (1999). We consider Tm clath a more appropriate physical-chemical parameter for the estimation of accurate salinity values, because, as discussed by Collins (1979), in aqueous-carbonic systems, part of the water is consumed during clathrate formation, thus increasing the salinity of the remaining liquid-phase, which exerts an influence on the accuracy of microthermometric measurements.

In general, the aqueous fluid inclusions yielded eutectic temperatures (Te) varying from -17.4º to -34.3ºC, although accurate measurements were relatively difficult to obtain. These data suggests that fluid inclusions are composed of H_2O and NaCl, with minor amounts of other dissolved ionic species such as Mg or K (Shepherd *et al.* 1985, Bodnar & Vityk 1994, Bodnar 1993). Tm ice values varied between -5.8º and -14.2ºC (Fig. 5A), corresponding to salinities ranging from 8 to 15 wt.% NaCl eq. Total homogenization temperature ($Th_{tot.}$) values varied between 332 and 474ºC (Fig. 5B), while total fluid density was estimated to be between 0.6 and 0.8 g/cm^{-3}. $Th_{tot.}$ was measured upon phase changes occurring in two ways:

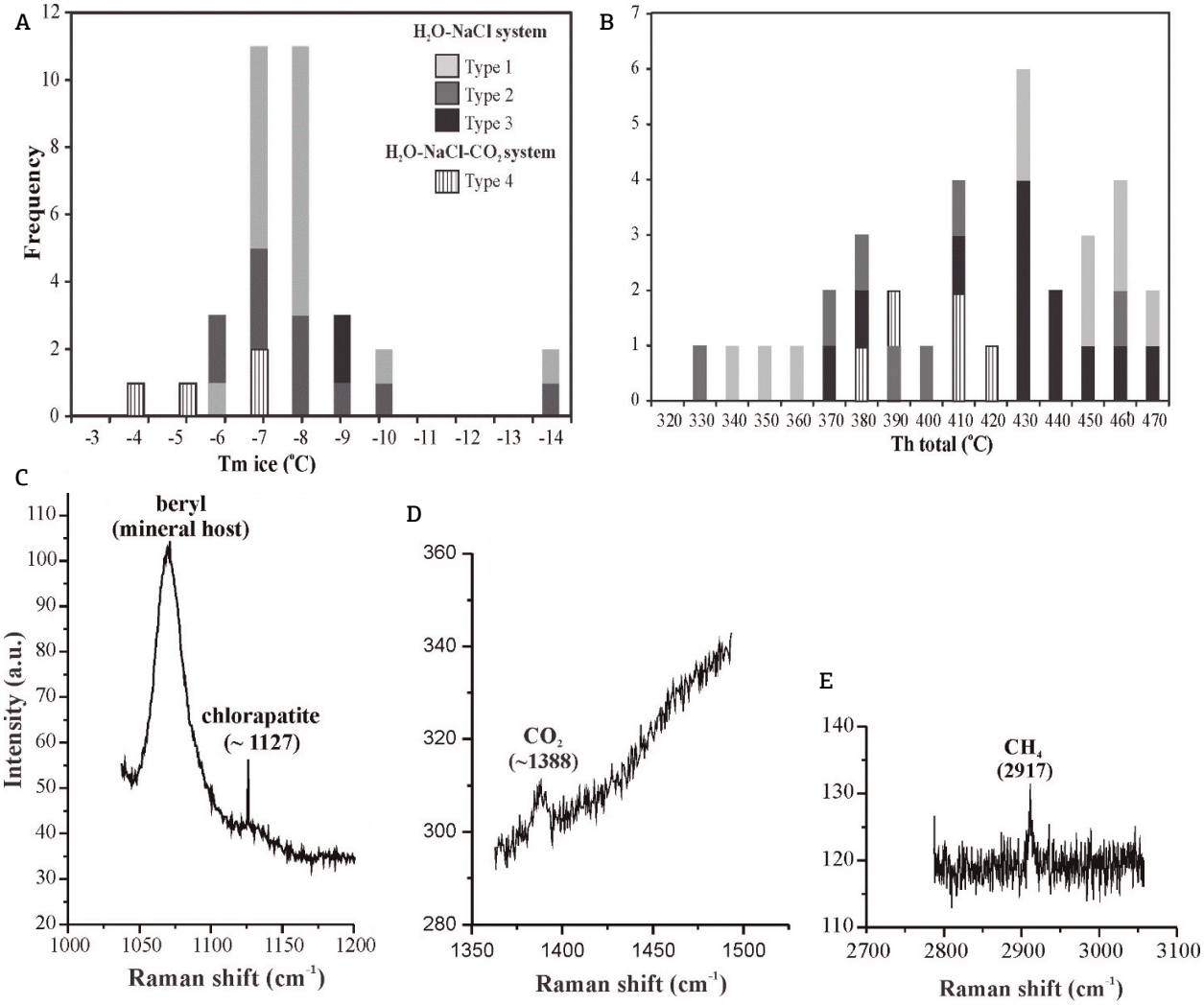

Figure 5. Frequency histograms showing the distributions of microthermometric data and Raman spectrum from emerald fluid inclusions. (A) Ice final melting temperatures (Tm ice); (B) total homogenization temperature ($Th_{tot.}$); (C) raman spectrum from aqueous fluid inclusions indicating to 1,127 cm^{-1} peak the chlorapatite ($Ca_5(PO_4)_3Cl$) as mineral captured; (D) Raman spectrum from aqueous-carbonic fluid inclusions indicating to 1,388 cm^{-1} and 2,917 cm^{-1} peaks the CO_2 and CH_4, respectively.

- contraction of the gas phase until blending into the liquid phase (LV → L, for fluid inclusions with Vg/Vt < 50%);
- disappearance of the liquid phase followed by expansion of the gas phase to fill completely the inclusion volume (LV → V, for fluid inclusions with Vg/Vt ≥ 50%).

In the latter case, the gas phase may contain small amounts of dissolved salts, therefore leading to inaccurate salinity and fluid density estimations using Tm ice values. Moreover, gas- and liquid-rich fluid inclusions co-existing in the H_2O-NaCl system suggest physical separation and subsequent heterogenization of trapped liquid-gas mixtures (*e.g.* Roedder 1984, Shepherd *et al.* 1985, Diamond 2003, Bodnar 2003).

Measurements of final melting temperatures of solid phases were not accomplished due to crepitation of several fluid inclusions at temperatures around 450ºC. Such situation leads to two different possible interpretations:

- final melting temperatures of solid phases are above 450ºC, probably around 500ºC, although morphological changes of solid phases indicating dissolution were not observed during heating steps;
- solid phases correspond to minerals captured during formation of cavities which were subsequently filled with liquid-gas mixtures.

Four birefringent solid daughter phases were sizable enough for investigation using micro Raman analysis. They showed peaks sustained at nearly 1,127 cm^{-1} (Fig. 5C), suggesting the presence of phosphates species, probably chlorapatite (Frezzotti *et al.* 2012). In addition, Zwaan *et al.* (2012) also identified carbonate, mica and bertrandite as captured minerals in fluid inclusion.

On the other hand, aqueous-carbonic fluid inclusions yielded solid CO_2 melting temperatures (Tm CO_2) between -56.9º and -56.7ºC, below the triple point of pure CO_2 (-56.6ºC). These data fall within the range of analytical error, so it is not possible to establish confidently whether the gas phase is composed of pure CO_2, or other gas species (*e.g.*, CH_4, N_2, H_2S) are also present in very low amounts along with CO_2 (Shepherd *et al.* 1985). During micro Raman analysis, only two fluid inclusions yielded responses indicating the presence of trace amounts of CH_4 associated with the CO_2 phase (Fig. 5D). The Tm ice was between -4.6 and -7.2ºC, and Tm clath ranged from 6.2 to 6.8ºC. Salinities calculated based on Tm clath vary from 6 to 7 wt.% NaCl eq. Partial homogenization of CO_2 (Th CO_2) in the liquid phase occurred between 24.2 and 25.8ºC, while total homogenization (Th tot.) was characterized by contraction and vibratory oscillation of the gas phase until it blended into the liquid phase between 383 and 424ºC (Fig. 5B). This fluid system had a total density calculated around 0.75 g/cm^3.

OXYGEN STABLE ISOTOPES

For oxygen isotope ($\delta^{18}O$) analysis, we selected three nearly pure emerald-quartz pairs from veinlets in apparent paragenetic association. Oxygen isotope ratios of the Fazenda Bonfim emeralds ($\delta^{18}O$ = 6.9–7.4‰, Tab. 2) are similar to those reported from other emerald deposits in Brazil ($\delta^{18}O$ = 6.8–12.2‰, in Giuliani *et al.* 1998). These isotopic ratios are also consistent with data from some other known emerald deposits worldwide ($\delta^{18}O$ = 6.2–12.1‰), characterized by interaction of fluids from two pre-existing rock types of contrasting geochemistry and isotopic signatures (Taylor Jr. 1978, Giuliani *et al.* 1997, 1998, Xue *et al.* 2010).

The oxygen isotope fractionation ratios ($\Delta\delta^{18}O$) of mineral pairs are normally used as geothermometers, applied to the different geological questions. In this context, $\delta^{18}O$ ratios of emerald-quartz pairs from the Bonfim deposit displayed little variations (Tab. 2), indicating relative isotopic equilibrium between minerals phases. However, the application of these data to estimate the isotopic fractionation temperature led us to obtain values between 746 and 573ºC for temperature emerald deposit formation (Tab. 2), using the empirically calibrated formula of Xue *et al.* (2010). This interval of isotopic temperature is far above of the total homogenization temperature interval (330–470ºC) obtained from fluid inclusion microthermometry. This temperature discrepancy may be due to some type of isotopic disequilibrium in the metasomatic environment, probably associated to fractionation during emerald/quartz growth or mixing with ^{18}O-depleted meteoric fluid. According to Giuliani *et al.*

Table 2. Oxygen isotopes ($\delta^{18}O$) data on the emerald and quartz from Fazenda Bonfim deposit. Observe the calculated values for the crystallization temperature ranges for the respective mineral pairs, using the empirically calibrated formula of Xue *et al.* (2010).

Mineral	$\delta^{18}O$ (‰)	$\Delta\ \delta^{18}O$ (‰) for mineral pairs (emerald + quartz)	Temperature range (ºC)
Emerald	6.8	0.3	746
Quartz	6.5		
Emerald	6.9	0.7	600
Quartz	6.2		
Emerald	7.4	0.8	573
Quartz	6.6		

(1998), isotopic variability is naturally related to the genesis of emerald in the metasomatic environment, which is interpreted to involve interaction of fluids with two pre-existing rocks of contrasting geochemistry and isotopic signatures, *i.e.*, Be-rich albite granite *vs* ultramafic rocks.

DISCUSSION

Several emerald deposits in the world were formed from metasomatic interactions between Be-rich granite intrusions and Cr(± V)-rich mafic-ultramafic rocks, which is referred to by other authors as "igneous model" (*e.g.*, Grundmann & Morteani 1989, Laurs *et al.* 1996, Schwarz & Giuliani 2001, Groat *et al.* 2002, Vapnik *et al.* 2006). In northeastern Brazil, the Fazenda Bonfim emerald is a good example of this metasomatic deposit type, with emerald crystals growing within the metasomatic phlogopite schist irregular level developed at the contact zone between Cr-rich mafic-ultramafic rocks from Archean-Paleoproterozoic basement (Seridó Group) and intrusive Be-rich albite-granite related to different generations or pulses during to Brasiliano orogeny (800–500 Ma). Geochronological analyses of albite-granite samples yielded a zircon U-Pb crystallization age of 561 ± 4 Ma, while metasomatic phlogopite schist ("blackwall" zone) samples yielded a mica Ar-Ar plateau age of 553 ± 4 Ma, indicating that the Fazenda Bonfim emeralds were formed at the end of the Brasiliano orogeny (Santiago 2017).

This metasomatic process involves reaction and permeability of a fluid advancing through lithological contacts, configuring a reaction front within rocks. Lithological contrast, temperature and pressure are factors that control the intensity of metasomatism. In general, the metasomatic front in mafic-ultramafic rocks is marked by development of "hornfels" phlogopite schist. At this site, there is addition of K, H, Li, Cs, Rb, Be, Al, and Na, and removal of Si, Mg, Ca, Fe, Cr, V and Sc. Nucleation and growth of emerald in phlogopite schist is the result of introduction of Be, Al and Na mobilized from pegmatite albite-granite, while Cr, Mg, Fe and V were released from mafic-ultramafic rocks and are responsible for emerald coloration (Laurs *et al.* 1996, Abdalla & Mohamed 1999, Alexandrov *et al.* 2001, Groat *et al.* 2008, Andrianjakavah *et al.* 2009).

The Fazenda Bonfim emerald crystals have chemical compositions characterized by high Mg and Na contents, having Cr as main chromophore element, followed by Fe and some V. In addition, trace amounts of Ca, K, Cs, Li, P, Sc, Ti, Mn, Co, Ni, Zn, Ga, and Rb are also found within emerald crystals. High Mg contents indicate formation in an Mg-rich environment (*i.e.*, phlogopite schist), due to beryl from pegmatites are normally very Mg poor (Grundmann & Morteani 1989, Sherriff *et al.* 1991, Artioli *et al.* 1993). These emerald crystals show concentric growth zones, as well as randomly-oriented mineral micro-inclusions, which indicates static growth. This zoning is probably linked to the cationic substitution of alkalis (mainly Na) in the octahedral site, besides variable degrees of Cr loss, which favors the crystals irregular coloration. This process is probably associated with some type of chemical imbalance present in the metasomatic environment (characterized by intense fluid-rock interaction) during growth of emerald crystals. According to Aurisicchio *et al.* (1988), zoning can occur as a result of chemical restrictions of the environment (bulk-rock chemistry and fluid-phase composition) or exchange reactions with other minerals present during growth of emerald, which can be, in turn, influenced by changes in pressure and temperature parameters.

Interestingly, a large amount of small emerald crystals with a size below 5 mm is observed in the Fazenda Bonfim deposit, indicating nucleation and subdued growth. This fact points for an intense, but not protracted, metasomatic process at along lithological contacts or distinct stages for emerald generation. Therefore, it is quite reasonable to infer some type of physical-chemical change or disequilibrium occurred during the evolution of this metasomatic environment, inhibiting the growth of part of the emerald crystals.

Studies of fluid inclusions from emerald crystals formed by igneous-metasomatic processes have determined variable compositions of low-density fluids corresponding either of $CO_2 \pm CH_4$-rich, H_2O- rich or mixed H_2O-$CO_2 \pm CH_4$ types, with salinities varying from low to moderate, and homogenization temperatures between 250 and 450ºC (*e.g.*, Alexandrov *et al.* 2001, Marshall *et al.* 2003, Vapnik *et al.* 2006, Xue *et al.* 2010, Lynch *et al.* 2014). In addition, oxygen isotope ratios ($\delta^{18}O$) from emerald crystals of this deposit type range from 5 to 11.5‰ (*e.g.*, Giuliani *et al.* 1997, 1998, Marshall *et al.* 2004, Groat *et al.* 2008, Marshall *et al.* 2012).

Fluid inclusion data from the Fazenda Bonfim emerald crystals revealed an essentially aqueous composition (H_2O + NaCl). Nevertheless, a $CO_2 \pm CH_4$ phase was also identified in very low concentrations. In general, this fluid system had low to moderate salinity (6–15 wt.% NaCl eq.), low density (0.6–0.8 g/cm^3) and total homogenization temperatures ranging from 330 to 470ºC. Microthermometry data obtained from aqueous phase-dominated fluid inclusions revealed different behaviors for the homogenization temperatures (*i.e.*, L + V → L and L + V → V). This characteristic, which is associated with presence of $CO_2 \pm CH_4$, might indicate "boiling" or "effervescence" assemblages involving physical separation with subsequent heterogenization trapped

liquid-gas mixtures, probably related to rapid changes in physical-chemical parameters (Wilkinson 2001, Bodnar 2003). However, this process has also leads to the very different range salinity on the residual fluid systems (Roedder 1984), but the fluid systems studied here showed salinity ranged from low to moderate. Mixed $H_2O + CO_2 \pm CH_4$ rare fluid system show a similar salinity to H_2O + NaCl dominant fluid system, indicating that the possible interaction with meteoric fluids (low salinity and light isotopically) has played a role, to a certain extent, during metasomatism fluid–rock.

H_2O-rich fluid phases have been linked to crustal origin, related to evolution and emplacement of fractionated granitic melts (*e.g.*, Bodnar 1995, Roedder & Bodnar 1997). On the other hand, the presence of CO_2 may be attributed to metamorphic devolatilization during to the Brasiliano orogeny (*e.g.*, Van der Kerkhof & Thiéry 2001), while that traces of CH_4, which have been reported in several emerald deposit (Vapnik *et al.* 2006), may be related to the oxygen fugacity during retrograde metamorphism conditions (*e.g.*, Van der Kerkhof *et al.* 1991). Therefore, it is reasonable to suggest that fluid phases coming from different sources have simultaneously interacted during the Fazenda Bonfim emerald growth. Thus, mixed fluid-phases played an important role in the mobility of ionic complex and ligands, transforming wall-rocks and altering their mineralogy (*e.g.*, Laurs *et al.* 1996, Schwarz & Giuliani 2001, Andrianjakavah *et al.* 2009).

Based on total homogenization temperature and salinity data obtained from types 1 and 2, aqueous phase-dominated fluid inclusions, we have calculated two isochores based on the experimental data of Bischoff (1991). These isochores were plotted along with the calibration curve for a fluid system with salinity of 15 wt.% NaCl eq. (Fig. 6), according to data by Bodnar (1993) and Bodnar and Vityk (1994). Such calibration curve was assumed by us to represent more closely the fluid system identified in this study, despite the low $CO_2 \pm CH_4$ contents. The isochores define an area ranging from 375 to 430ºC, and from 200 to 600 bars, with the latter figures corresponding to burial depths ranging from 2 to approximately 5 km, compatible with greenschist to low-amphibolite metamorphic facies. This is also in reasonably good agreement with conditions for evolved alkaline-granitoids/pegmatites generated during late stages of the Brasiliano Orogeny (Silva *et al.* 1995, Araújo *et al.* 2001, Guimarães *et al.* 2000, Santos *et al.* 2008, Beurlen *et al.* 2009).

Fluid inclusion and oxygen isotope data have been combined to obtain pressure and temperature estimates of fluid entrapment conditions for some emerald deposits (*e.g.*, Giuliani *et al.* 1997, Marshall *et al.* 2003, Xue *et al.* 2010, Marshall *et al.* 2012). However, in the Fazenda Bonfim emerald deposit, the isotopic temperature range for

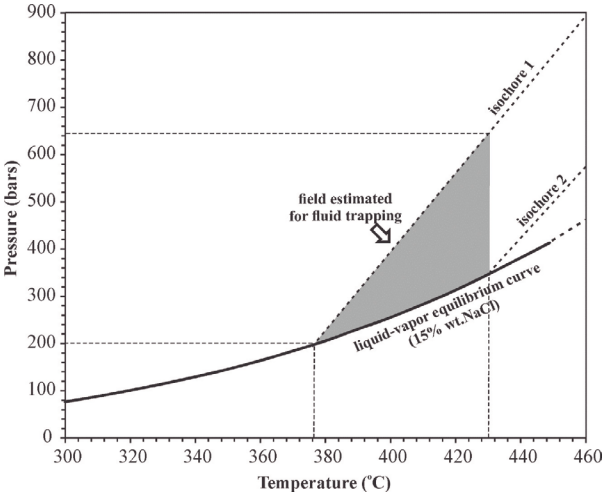

Figure 6. P-T diagram showing estimated conditions for fluid trapping and emerald mineralization at Fazenda Bonfim deposit (shaded area). Isochore 1 (type 1 fluid inclusion) was calculated based on Th = 375ºC and salinity = 18 wt.% NaCl eq., while isochore 2 (type 2 fluid inclusion) was calculated based on Th = 430ºC and salinity = 10 wt.% NaCl eq.

quartz–emerald pairs (746–573ºC) is above the trapping temperature range defined by fluid inclusion isochores. This may be due to some degree of disequilibrium in the ^{18}O distribution of quartz-emerald pairs within the metasomatic environment (Giuliani *et al.* 1998). On the other hand, the hexagonal crystalline structure of beryl has channels parallel to the *c* axis where water and some cations, that can to a certain extent contribute to the overall $\delta^{18}O$ signatures, are accommodated (Taylor *et al.* 1992, Groat *et al.* 2008, Marshall *et al.* 2012). It is also possible that heavy mineral (zircon, monazite and others) micro-inclusions identified within emerald crystals can produce subtle variations in the oxygen isotope composition. Nevertheless, oxygen isotope ratios from Fazenda Bonfim emerald crystals are consistent with those from other deposits formed by igneous-metasomatic process (Giuliani *et al.* 1997, 1998).

CONCLUDING REMARKS

The data presented in this study, combined with data available from literature, led to the following conclusions:

- the Fazenda Bonfim emerald deposit was formed at the end of the Brasiliano orogeny (~ 553 Ma years ago) as a result of intense, but not protracted, metasomatic process (*i.e.*, igneous model or type-I, according to Schwarz & Giuliani 2001) that took place along lithological contacts between Be-rich albite-granite intrusions and Cr (± V)-rich mafic-ultramafic host-rocks. Nucleation and growth of

emerald crystals occurred approximately in static mode within "hornfels" phlogopite schist ("blackwall" zone), controlled by entrance of Be, Al and Na (mobilized from albite-granite), while Cr, Mg, Fe and V released from mafic-ultramafic wall-rocks were responsible for emerald color. Otherwise, the differences in size of the emerald crystals suggest distinct stages of nucleation and growth;

- emerald crystals show relatively high contents of Mg and Na, as well as trace amounts of Ca, K, Cs, Li, P, Sc, Ti, Mn, Co, Ni, Zn, Ga and Rb. Cr is the main chromophore element, followed by Fe and, to a lesser extent, V. Crystals also exhibit discreet concentric growth zones produced by cationic substitution of alkalis in the octahedral sites, whose mechanism is main responsible for changes of color toward pale green hues, with Cr losses. Although the cause of this type of zoning is not yet clear, we believe that some chemical imbalance or variation in physical-chemical conditions of the metasomatic environment (*e.g.*, bulk-rock chemistry and fluid-phase composition, associated with variations in pH, Eh, P and T) are likely to be the main factors;
- metasomatic fluids contemporaneous with emerald growth have compositions of essentially aqueous type (H_2O + NaCl), with low to moderate salinity and low density, although trace amounts of $CO_2 \pm CH_4$ were also observed. This fluid system had an important role in cation transferring and was marked by phase separation (*i.e.*, boiling or effervescence processes) and mixture (*i.e.*, hydrothermal *vs* meteoric fluids), with subsequent heterogeneous trapping of liquid-gas mixtures. Fluids were trapped mostly between 375 and 430ºC, and 200 and 600 bars, based on combination of fluid inclusion isochores. In addition, oxygen isotope data ($\delta^{18}O$ = 6.9–7.4‰) suggest an igneous-metasomatic source for fluids and emerald components.

ACKNOWLEDGEMENTS

This research had financial support from the Brazilian National Council of Technological and Scientific Development (CNPq - Project n. 308312/2014/7) and Geology Postgraduate Program of the University of Brasília. We thank the Brazilian Coordination for Improvement of Higher Education Personnel (CAPES) for the scholarship granted to the first author. The authors are also grateful to geologist Luiz Rodrigues Neto (Nosso Senhor do Bonfim Mining Company) for his support during fieldwork. Special thanks are offered to anonymous reviewers whose comments helped improve the final version of the manuscript.

REFERENCES

Abdalla H.M. & Mohamed F.H. 1999. Mineralogical and geochemical investigation of emerald and beryl mineralisation, Pan-African Belt of Egypt: genetic and exploration aspects. *Journal of African Earth Sciences*, **28**:581-598. https://doi.org/10.1016/S0899-5362(99)00033-0

Agrawal V.N. 1992. Relations between pegmatite emplacements and tectono-metamorphic events in the Seridó Group, northeastern Brazil. *Revista Brasileira de Geociências*, **22**(l):43-46.

Alexandrov P., Giuliani G., Zimmermann J-L. 2001. Mineralogy, age and fluid geochemistry of the Rila emerald deposit, Bulgaria. *Economic Geology*, **96**:1469-1476. https://doi.org/10.2113/gsecongeo.96.6.1469

Almeida F.F.M., Hasui Y., Brito Neves B.B., Fuck R.A. 1981. Brazilian structural provinces: an introduction. *Earth-Science Reviews*, **17**(1-2):1-29. https://doi.org/10.1016/0012-8252(81)90003-9

Andrianjakavah P.R., Salvi S., Béziat D., Rakotondrazafy M., Giuliani G. 2009. Proximal and distal styles of pegmatite-related metasomatic emerald mineralization at Ianapera, southern Madagascar. *Mineralium Deposita*, **44**:817-835. http://dx.doi.org/10.1007/s00126-009-0243-5

Angelim L.A.A., Nesi J.R., Torres H.H.F., Medeiros V.C., Santos C.A., Junior J.P.V., Mendes V.A. 2006. *Geological and Mineral Resources of the State of Rio Grande do Norte Project*. Geology of Brazil Program (PGB). Geological Mapping, 1:500.000 scale. Recife (Brazil), MME-FAPERN, 76 p.

Araújo M.N.C., Alves da Silva F.C., Jardim de Sá E.F. 2001. Pegmatite Emplacement in the Seridó Belt, Northeastern Brazil: Late Stage Kinematics of the Brasiliano Orogen. *Gondwana Research*, **4**(1):75-85. https://doi.org/10.1016/S1342-937X(05)70656-0

Artioli G., Rinaldi R., Stahl K., Zanazzi P.F. 1993. Structure refinements of beryl by single-crystal neutron and X-ray diffraction. *American Mineralogist*, **78**:762-768.

Aurisicchio C., Fioravanti O., Grubessi O., Zanazzi P.F. 1988. Reappraisal of the crystal chemistry of beryl. *American Mineralogists*, **73**:826-837.

Bakker R.J. 1999. Adaptation of the Bowers and Helgeson (1983) equation of state to the H_2O-CO_2-CH_4-NaCl system. *Chemical Geology*, **154**:225-236. DOI: 10.1016/S0009-2541(98)00133-8

Baumgartner R., Rolf L., Romer R.L., Moritz R., Sallet R., Chiaradia M. 2006. Columbite-tantalite-bearing granitic pegmatites from the Seridó Belt, northeastern Brazil: genetic constraints from U-Pb dating and Pb isotopes. *Canadian Mineralogist*, **44**(1):69-86. https://doi.org/10.2113/gscanmin.44.1.69

Beurlen H., Barreto S., Martin R., Melgarejo J., Rhede D., Silva M.R.R., Souza Neto J. 2009. The Borborema Pegmatitic Province, NE-Brazil revisited. *Estudos Geológicos*, **19**(2):62-66. DOI: 10.18190/1980-8208/estudosgeologicos.v19n2p62-66

Beurlen H., Silva M.R.R., Castro C. 2001. Fluid inclusion microthermometry in Be-Ta-(Li-Sn)-bearing pegmatites from the Borborema Province, northeastern Brazil. *Chemical Geology*, **173**(1-3):107-123. https://doi.org/10.1016/S0009-2541(00)00270-9

Bischoff J.L. 1991. Densities of liquids and vapors in boiling NaCl-H_2O solutions: A PVTX summary from 300º-500ºC. *American Journal of Science*, **291**:309-338.

Bodnar R.J. 1993. Revised equation and table determining the freezing point depression of H_2O-NaCl solutions. *Geochimica et Cosmochimica Acta*, **57**:683-684. DOI: 10.1016/0016-7037(93)90378-A

Bodnar R.J. 1995. Fluid inclusion evidence for a magmatic source for metals in porphyry copper deposits. *In:* Thompson J.F.H. (ed.). *Magmas, Fluids and Ore Deposits: short course*. Canada, Mineralogical Association of Canada, v. 23, p. 39-152.

Bodnar R.J. 2003. Introduction to fluid inclusions. *In*: Samson, A. A. & Marshall D. (eds.), *Fluid Inclusions:* Analysis and Interpretation. Short Course. Vancouver, Mineralogical Association Canada, v. 32, p. 1-8.

Bodnar R.J. & Vityk M.O. 1994. Interpretation of microthermometric data for H_2O-NaCl fluid inclusions. *In:* Vivo B. De & Frezzotti M.L. (eds.), *Fluid Inclusions in Minerals:* Methods and Applications. Short course of the working group (IMAQ) "Inclusions in Minerals". Pontignano, Siena, p. 117-130.

Brasil. Ministério da Indústria, Comércio Exterior e Serviços. 2017. *Internet information system*. Available from: <http://aliceweb.desenvolvimento.gov.br/>. Accessed on: 08/20/2017.

Brito Neves B.B., Fuck R.A., Pimentel M.M. 2014. The Brasiliano collage in South America: a review. *Brazilian Journal of Geology*, **44**(3):493-518. http://dx.doi.org/10.5327/Z2317-4889201400030010

Brito Neves B.B., Santos E.J., Van Schmus W.R. 2000.The tectonic history of the Borborema Province. *In:* Cordani U.G., Milani E.J., Thomaz Filho A., Campos D.A. (eds.), *Tectonic evolution of South America*. Rio de Janeiro, 31st International Geological Congress, **2**:151-182.

Brown P.E. & Hagemann S.G. 1994. MacFlinCor: A computer program for fluid inclusion data reduction and manipulation. *In:* ViVo B. & Frezzotti M.L. (eds.), *Fluid Inclusions in Minerals:* Methods and Applications. Short course of the working group (IMAQ) "Inclusions in Minerals". Pontignano, Siena, p. 231-250.

Caby R., Arthaud M., Archanjo C.J. 1995. Lithostratigraphy and petrostructural characterization of supracrustal units in the Brasiliano Belt of Northeastern Brazil: geodynamic implications. *Journal of South American Earth Sciences*, **8**(3-4):235-246.

Caby R., Sial A.N., Arthaud M., Vauchez A. 1991. Crustal evolution and the Brasiliano orogeny in Northeast Brazil. *In:* Dallmeyer R.D. & Lécorché J.C.P.L. (eds.), *The West African Orogens and Circum-Atlantic Correlatives*. Berlin, Springer Verlang, p. 373-397.

Cassedanne J.P. 1991. Brazilian gemstones typology. *In:* Schobbenhaus C., Queiroz E.T., Coelho C.E.S. (eds.). *Main Brazilian Mineral Deposits*. Brasília, DNPM/CPRM, v. 4, p. 17-36.

Cavalcante R., Cunha A.L.C., Oliveira R.G., Medeiros V.C., Dantas A.R., Costa A.P., Lins C.A.C., Larizzatti J.H. 2016. *Metalogenesis of the Brazilian Mineral Provinces:* east Seridó area, northeastern Borborema Province (Rio Grande do Norte and Paraíba states). Brazil: Geology of Brazil Program (PGB), MME-SGB/CPRM (Brazil), Brazilian Minerals Provinces Series, n. 8, 103 p.

Cavalcanti Neto M.T.O. & Barbosa R.V.N. 2007. The emeralds from Lajes, Caiçara do Rio dos Ventos and São Tomé/RN. *Holos*, **2**:92-104.

Collins P.L. 1979. Gas hydrates in CO_2-bearing fluid inclusions and the use of freezing data for estimation of salinity. *Economic Geology*, **74**(6):1435-1444. https://doi.org/10.2113/gsecongeo.74.6.1435

Dantas E.L. 1997. *U/Pb and Sm/Nd geocronology of the Archean and Paleoproterozoic terraine from São José do Campestre Massif, NE Brazil*. PhD Thesis, Geoscience Institute, Universidade Estadual Paulista "Júlio de Mesquita Filho", Rio Claro, São Paulo, 211p.

Dantas E.L., Souza Z.S., Wernick E., Hackspacher P.C., Martin H., Xiaodong D., Li J.-W. 2013. Crustal growth in the 3.4–2.7 Ga São José de Campestre Massif, Borborema Province, NE Brazil. *Precambrian Research*, **227**:120-156. https://doi.org/10.1016/j.precamres.2012.08.006

Diamond L.W. 1992. Stability of CO_2 clathrate hydrate+ CO_2 liquid+ CO_2 vapour + aqueous KCl-NaCl solutions: Experimental determination and application to salinity estimates of fluid inclusions. *Geochimica et Cosmochimica Acta*, **56**(1):273-280. https://doi.org/10.1016/0016-7037(92)90132-3

Diamond L.W. 2003. Systematics of H_2O inclusions. *In:* Samson I., Anderson A., Marshall D. (eds.). *Fluid inclusions analysis and interpretation*. Short Course Series. Canada, Mineralogical Association of Canada, v. 32, p. 55-79.

Ferraris G., Prencipe M., Rossi P. 1998. Stoppaniite, a new member of the beryl group: crystal structure and crystal-chemical implications. *European Journal of Mineralogy*, **10**:491-496.

Ferreira V.P., Sial A.N., Jardim de Sá E.F. 1998. Geochemical and isotopic signatures of Proterozoic granitoids in terrenes of the Borborema structural province, northeastern Brazil. *Journal of South America Earth Sciences*, **11**(5):439-455. https://doi.org/10.1016/S0895-9811(98)00027-3

Frezzotti M.L., Tecce F., Casagli A. 2012. Raman spectroscopy for fluid inclusion analysis. *Journal of Geochemical Exploration*, **112**:1-20. https://doi.org/10.1016/j.gexplo.2011.09.009

Gibbs G.V., Breck D.W., Meagher E.P. 1968. Structural refinement of hydrous and anhydrous synthetic beryl $A1_2Be_3$, Si_6, O_{18}, $Al_{1.9}$, and emerald, $Cr_{0.1}$, Be_3, Si_6, O_{18}. *Lithos*, **1**:275-285. https://doi.org/10.1016/S0024-4937(68)80044-1

Giuliani G., France-Lanord C., Coget P., Schwarz D., Cheilletz A., Branquet Y., Giard D., Martin-Izard A., Alexandrov P., Piat D.H. 1998. Oxygen isotope systematics of emerald: Relevance for its origin and geological significance. *Mineralium Deposita*, **33**:513-519. DOI: 10.1007/s001260050166.

Giuliani G., France-Lanord C., Zimmerman J.L., Cheilletz A., Arboleda C., Charoy B., Coget P., Fontan F., Giard D. 1997. Fluid composition, δD of channel H_2O and $\delta^{18}O$ of lattice oxygen in beryls: Genetic implications for Brazilian, Colombian, and Afghanistani emerald deposits. *International Geology Review*, **39**:400-424. DOI: 10.1080/00206819709465280

Giuliani G., Silva L.J.H.D., Couto P. 1990. Origin of emerald deposits of Brazil. *Mineralium Deposita*, **25**:57-64. DOI: 10.1007/BF03326384

Groat L.A, Giuliani G., Marshall D.D., Turner D. 2008. Emerald deposits and occurrences: A review. *Ore Geology Reviews*, **34**:87-112. https://doi.org/10.1016/j.oregeorev.2007.09.003

Groat L.A., Marshall D.D., Giuliani G., Murphy D.C., Piercey S.J., Jambor J.L., Mortensen J.K., Ercit T.S., Gault R.A., Mattey D.P., Schwarz D., Maluski H, Wise M.A., Wengzynowski W., Eaton D.W. 2002. Mineralogical and geochemical study of the Regal Ridge Emerald Showing, Southeastern Ukon. *The Canadian Mineralogist*, **40**:1313-1338. https://doi.org/10.2113/gscanmin.40.5.1313

Grundmann G. & Morteani G. 1989. Emerald mineralization during regional metamorphism: the Habachtal (Austria) and Leydsdorp (Transvaal, South Africa) deposits. *Economic Geology*, **84**(7):1835-1849. https://doi.org/10.2113/gsecongeo.84.7.1835

Guimarães I.P., Almeida C.N., Silva Filho A.F., Araújo J.M.M. 2000. Granitoids marking the end of the Brasiliano (Pan-African) orogeny within the central tectonic domain of the Borborema Province. *Revista Brasileira de Geociências*, **30**(1):177-181.

Jardim de Sá E.F. 1994. *Seridó Mobile Belt (Borborema Province, NE Brazil) and its geodynamic meaning in the Brasiliano/Pan-African cycle*. PhD Thesis, Instituto de Geociências, Universidade de Brasília, Brasília, 803 p.

Jardim de Sá E.F., Fuck R.A., Macedo M.H.F., Peucat J.J., Kawashita K., Souza Z.S., Bertrandt J.M. 1995. Pre-Brasiliano orogenic evolution in the Seridó Belt, NE Brazil: conflicting geochronological and structural data. *Revista Brasileira de Geociências*, **25**(4):307-314.

Jardim de Sá E.F., Legrand J.M., McReath I. 1981. Stratigraphy of granitoid rocks in the Seridó region (RN-PB): Based on structural criteria. *Revista Brasileira de Geociências*, **11**:50-57.

Johnston Jr. W.D. 1945. Beryl-tantalite pegmatite of northeastern Brazil. *Geological Society of American Bulletin*, **56**:1015-1070. https://doi.org/10.1130/0016-7606(1945)56[1015:BPONB]2.0.CO;2

Laurs B.M., Dilles J.H., Snee L.W. 1996. Emerald mineralization and metasomatism of amphibolite, Khaltaro granitic pegmatite - hydrothermal vein system, Haramosh Mountains, northern Pakistan. *The Canadian Mineralogist*, **34**:1253-1286.

Lynch E.P., Costanzo A., Feely M., Blamey N.J.F., Pironon J., Lavin P. 2014. The Piteiras emerald mine, Minas Gerais, Brazil: fluid-inclusion and gemological perspectives. *Mineralogical Magazine*, **78**(7):1571-1587. https://doi.org/10.1180/minmag.2014.078.7.04

Marshall D., Downes P.J., Ellis S., Greene R., Loughrey L., Jones P. 2016. Pressure–temperature–fluid constraints for the Poona emerald deposits, Western Australia: fluid inclusion and stable isotope studies. *Minerals*, **6**(4):130. http://dx.doi.org/10.3390/min6040130

Marshall D., Groat L., Falck H., Giuliani G., Neufeld H. 2004. The Lened emerald prospect, Northwest Territories, Canada: insights from fluid inclusions and stable isotopes, with implications for northern cordilleran emerald. *The Canadian Mineralogist*, **42**:1523-1539. DOI: 10.2113/gscanmin.42.5.1523

Marshall D., Groat L., Giuliani G., Murphy D., Mattey D., Ercit T.S., Wise M.A., Wengzynowski W., Eaton W.D. 2003. Pressure, temperature and fluid conditions during emerald precipitation, southeastern Yukon, Canada: fluid inclusion and stable isotope evidence. *Chemical Geology*, **194**:187-199. https://doi.org/10.1016/S0009-2541(02)00277-2

Marshall D., Pardieu V., Loughrey L., Jones P., Xue G. 2012. Conditions for emerald formation at Davdar, China: fluid inclusion, trace element and stable isotope studies. *Mineralogical Magazine*, **76**(1):213-226. https://doi.org/10.1180/minmag.2012.076.1.213

Morosin B. 1972. Structure and thermal expansion of beryl. *Acta Crystallographica*, **28**:1899-1903. https://doi.org/10.1107/S0567740872005199

Nascimento M.A.L., Antunes A.F., Galindo A.C., Ferraz E., Jardim de Sá E.F., Souza Z.S. 2000. Geochemical Signature of the Brasiliano-Age Plutonism in the Seridó Belt, Northeastern Borborema Province (NE Brazil). *Revista Brasileira de Geociências*, **30**(1):161-164.

Neves S.P. 2003. Proterozoic history of the Borborema Pronvince (NE Brazil): Correlation with neighboring cratons and Pan-African belts and implications for the evolution of western Gondwana. *Tectonics*, **22**(4):5-14. DOI: 10.1029/2001TC001352

Oliveira J.A.P. & Ali S.H. 2011. Gemstone mining as a development cluster: a study of Brazil's emerald mines. *Resources Policy*, **36**:132-141. https://doi.org/10.1016/j.resourpol.2010.10.002

Roedder E. 1984. Fluid inclusions. *In:* Ribbe P.H. (ed.), *Reviews in Mineralogy*. Mineralogical Society of America, vol. 12, 644 p.

Roedder E. & Bodnar R.J. 1997. Fluid inclusions studies of hydrothermal ore deposits. *In*: Barnes H.L. (ed.). *Geochemistry of Hydrothermal Ore Deposits*. 3ª ed. New York, John Wiley CO., p. 657-697.

Sampaio Filho H.A., Sighnolfi G.P., Galli E. 1973. Contribution to the crystal chemistry of beryl. *Contribution to Mineralogy and Petrology*, **38**:279-290.

Santiago J.S. 2017. *Emerald mineralization during the Brasiliano Orogeny in northeastern Brazil: The case of the Fazenda Bonfim deposit, State of Rio Grande do Norte*. Masters Dissertation, Programa de Pós-Graduação em Geologia, Instituto de Geociências, Universidade de Brasília, Brasília, 32 p.

Santos T.J.S., Fetter A.H., Hackspacher P.C., Van Schmus W.R., Nogueira Neto J.A. 2008. Neoproterozoic tectonic and magmatic episodes in the NW sector of Borborema Province, NE Brazil, during assembly of Western Gondwana. *Journal of South American Earth Sciences*, **25**:271-284. https://doi.org/10.1016/j.jsames.2007.05.006

Scholz R., Romano A.W., Belotti F.M., Chaves M.L.S.C. 2010. Geochemical prospection of beryl emerald variety in the Fazenda Bonfim region (Lajes, RN). *Geociências*, **29**(4):613-621.

Schwarz D. 1987. *Emeralds: inclusions in gens*. Universidade Federal de Ouro Preto, Ouro Preto, Brazil, 439p.

Schwarz D. & Giuliani G. 2001. Emerald deposits a review. *The Australian Gemmologist*, **21**:17-23.

Sharp Z.D. 1990. A laser-based microanalytical method for the in situ determination of oxygen isotope ratios of silicates and oxides. *Geochimica et Cosmochimica Acta*, **54**:1353-1357. https://doi.org/10.1016/0016-7037(90)90160-M

Shepherd T.J., Rankin A.H., Alderton D.H.M. 1985. *A practical guide to fluid inclusion studies*. New York, Chapman and Hall, 239 p.

Sherriff B.L., Grundy D.H., Hartman J.S, Hawthorne F.E., Cerny P. 1991. The incorporation of alkalis in beryl: Multi-nuclear MASNMR and crystal structure study. *Canadian Mineralogist*, **29**:271-285.

Sial A.N. 1986. Granite-types in northeast Brazil: current knowledge. *Revista Brasileira de Geociências*, **16**(1):54-72.

Silva M.R.R., Höll R., Beurlen H. 1995. Borborema Pegmatite Province: geological and geochemical characteristics. *Journal of South American Earth Sciences*, **8**(3-4):355-364. https://doi.org/10.1016/0895-9811(95)00019-C

Souza Z.S., Martin H., Peucat J.J., Jardim de Sá E.F., Macedo M.H.F. 2007. Calcalkaline magmatism at the Archean-Proterozoic transition: the Caicó complex basement (NE Brazil). *Journal of Petrology*, **48**:2149-2185.

Souza Neto J.A., Legrand J.M., Volfinger M., Pascal M.-L., Sonnet P. 2008. W–Au skarns in the Neo-Proterozoic Seridó Mobile Belt, Borborema Province in northeastern Brazil: an overview with emphasis on the Bonfim deposit. *Mineralium Deposita*, **43**:185-205. DOI: 10.1007/s00126-007-0155-1

Taylor R.P., Fallick A.E., Breaks F.W. 1992. Volatile evolution in Archean rare-element granitic pegmatites; evidence from the hydrogen isotopic composition of channel H_2O in beryl. *Canadian Mineralogist*, **30**:877-893.

Taylor Jr. H.P. 1978. Oxygen and hydrogen isotope studies of plutonic granitic rocks. *Earth and Planetary Science Letters*, **38**:177-210. https://doi.org/10.1016/0012-821X(78)90131-0

Van der Kerkhof A. & Thiéry R. 2001. Carbonic inclusions. *Lithos*, **55**:49-68. https://doi.org/10.1016/S0024-4937(00)00038-4

Van der Kerkhof A.M., Touret J.L.R., Maijer C., Jansen J.B.H. 1991. Retrograde methane-dominated fluid inclusions from high-temperature granulites of Rogaland, southwestern Norway. *Geochimica et Cosmochimica Acta*, **55**:2533-2544. https://doi.org/10.1016/0016-7037(91)90371-B

Van Schmus W.R., Brito Neves B.B., Hackspacher P., Babinski M. 1995. UPb and SmNd geochronolgic studies of eastern Borborema Province, northeastern Brazil: initial conclusions. *Journal of South American Earth Sciences*, **8**(3-4):267-288. https://doi.org/10.1016/0895-9811(95)00013-6

Van Schmus W.R., Brito Neves B.B., Williams I.S., Hackspacher P., Fetter A.H., Dantas E.L., Babinski M. 2003. The Seridó Group of NE Brazil, a late Neoproterozoic pre- to syn-collisional basin in West Gondwana: insights from SHRIMP U–Pb detrital zircon ages and Sm–Nd crustal residence (TDM) ages. *Precambrian Research*, **127**:287-327. DOI: 10.1016/S0301-9268(03)00197-9

Vapnik Y.E., Moroz I., Roth M., Eliezri I. 2006. Formation of emeralds at pegmatite-ultramafic contacts based on fluid inclusions in Kianjavato emerald, Mananjary deposits, Madagascar. *Mineralogical Magazine*, **70**(2):141-158. https://doi.org/10.1180/0026461067020320

Wilkinson J.J. 2001. Fluid inclusions in hydrothermal ore deposits. *Lithos*, **55**(1-4):229-272. https://doi.org/10.1016/S0024-4937(00)00047-5

Xue G., Marshall D., Zhang S., Ullrich T.D., Bishop T., Groat L.A., Thorkelson D.J., Giuliani G., Fallick A.E. 2010. Conditions for early Cretaceous emerald formation at Dyakou, China: fluid inclusion, Ar-Ar, and stable isotope studies. *Economic Geology*, **105**:339-349. https://doi.org/10.2113/gsecongeo.105.2.339

Zwaan J.C.H., Jacob D.E., Häger T., Cavalcanti Neto M.T.O., Kanis J. 2012. Emeralds from the Fazenda Bonfim region, Rio Grande do Norte, Brazil. *Gems & Gemology*, **48**(1):2-17. DOI: 10.5741/GEMS.48.1.2.